

(LACK OF) LENSING CONSTRAINTS ON CLUSTER DARK MATTER PROFILES

NEAL DALAL¹

Institute for Advanced Study, Einstein Drive, Princeton, NJ 08540

CHARLES R. KEETON¹

Astronomy & Astrophysics Department, University of Chicago, 5640 S. Ellis Ave., Chicago, IL 60637

Draft version June 27, 2018

ABSTRACT

Using stellar dynamics and strong gravitational lensing as complementary probes, Sand et al. (2002, 2003) have recently claimed strong evidence for shallow dark matter density profiles in several lensing clusters, which may conflict with predictions of the Cold Dark Matter paradigm. However, systematic uncertainties in the analysis weaken the constraints. By re-analyzing their data, we argue that the tight constraints claimed by Sand et al. were driven by prior assumptions. Relaxing the assumptions, we find that no strong constraints may be derived on the dark matter inner profile from the Sand et al. data; we find satisfactory fits (with reasonable parameters) for a wide range of inner slopes $\rho \propto r^{-\beta}$ with $0 < \beta < 1.4$. Useful constraints on the mass distributions of lensing clusters can still be obtained, but they require moving beyond mere measurements of lensing critical radii into the realm of detailed lens modeling.

Subject headings: gravitational lensing — dark matter — galaxies: clusters — galaxies: clusters: individual (Abell 383, MS 2137–23)

1. COLD DARK MATTER OR CORED DARK MATTER?

The central density profile of dark matter halos has been the subject of considerable debate in recent years. On the theoretical side, numerous groups have claimed that dissipationless N-body simulations in the Cold Dark Matter (CDM) model produce universal halo profiles. Despite vigorous debate over the exact shape of the inner profile, there is general agreement that predicted CDM halos have central density cusps, $\rho \propto r^{-\beta}$ with $\beta \sim 1$ –1.5 (e.g., Moore et al. 1998; Navarro et al. 1997, 2003). On the observational side, similar controversy has raged over the question of whether such cusps are present in real galaxies, and whether their absence would challenge the CDM paradigm (e.g., Dutton et al. 2003; Simon et al. 2003, and references therein). The most difficult issue is accounting for the effects of baryonic matter, which contributes directly to the gravitational potential and may also modify the dark matter distribution (e.g., Blumenthal et al. 1986; El-Zant et al. 2003; Loeb & Peebles 2003).

Strongly lensed arcs in galaxy clusters probe the gravitational potential on scales ($r \sim 50$ –100 kpc) large enough to avoid significant baryonic contamination, and hence can provide a relatively clean test of the predictions of dissipationless N-body simulations. Several groups have constrained the density profiles of individual clusters by studying their lensing properties (Athreya et al. 2002; Clowe & Schneider 2002; Dahle 2003), and in some cases have obtained stringent limits from combined strong- and weak-lensing analyses (e.g., Gavazzi et al. 2003; Kneib et al. 2003).

Another approach is to disentangle the baryonic and dark matter contributions to the net potential on small scales, similar to studies of galaxy rotation curves.

Kelson et al. (2002) have used the velocity dispersion profile of the cD galaxy in the cluster Abell 2199 together with the kinematics of the cluster members to decompose the stellar and dark matter components. They found that a $\beta = 1.5$ dark matter cusp is ruled out by the velocity dispersion data, while a $\beta = 1$ cusp is difficult to reconcile with a reasonable mass-to-light ratio for the cD galaxy. Sand et al. (2002, 2003, hereafter S03) have gone a step further and combined dynamical and strong lensing analyses for six clusters. Two of their clusters provide particularly tight and interesting results: inner slopes of $\beta = 0.57 \pm 0.11$ for MS 2137–23 and $\beta = 0.38 \pm 0.06$ for Abell 383, which strongly conflict with the steep cusps predicted for CDM. Such a conflict on cluster scales may be more troubling than similar conflicts on galaxy scales, as there are fewer proposed processes that are capable of disrupting dark matter cusps in clusters.

The S03 results are somewhat puzzling, however, as illustrated in Figure 1. This figure shows velocity dispersion profiles and representative lensed arcs for three models of Abell 383: the best-fit model found by S03, a model with a $\beta = 1$ dark matter cusp, and a model with $\beta = 0$. While the fit with a $\beta = 1$ cusp is by no means perfect, it is clearly not ruled out at the 10- σ level (as claimed by S03). Moreover, it is not significantly worse than the best-fit model presented by S03.

In this paper we study the origin of this discrepancy. We argue that the tight constraints claimed by S03 result from assumptions made in their modeling. In particular, they assumed spherical symmetry and adopted particular values for the scale radius at which the dark matter density profile transitions from $r^{-\beta}$ to r^{-3} . Relaxing these assumptions, we find that no interesting constraints on the dark matter profile can be derived from the S03 data alone. However, more detailed modeling of the lensing properties of these clusters may yield stronger

¹ Hubble Fellow

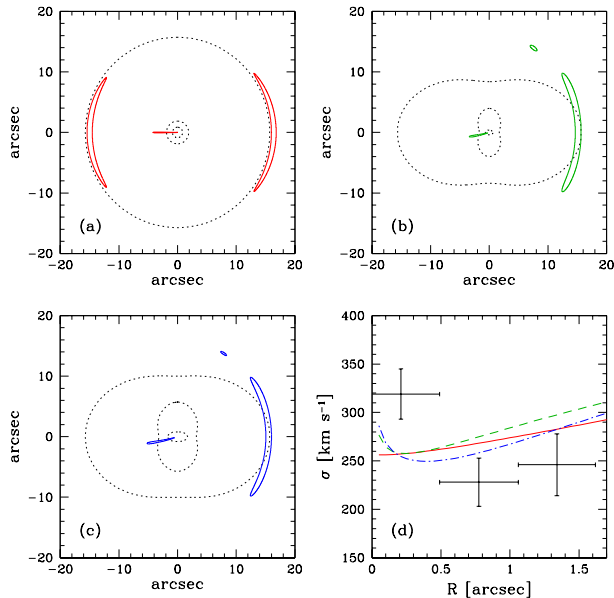


FIG. 1.— (a–c) Representative model arcs for Abell 383. The model parameters are listed in Table 1. The solid curves show the arcs, while the dotted curves show the lensing critical curves. Model a is the best-fit model from S03; the second tangential arc is an artifact of the assumed spherical symmetry. In models b and c, the arclet near the tangential arc is a predicted counter-image of the radial arc. (d) Velocity dispersion profiles for models a (solid line), b (dashed line), and c (dash-dot line), compared with the data from S03.

TABLE 1. SAMPLE MODEL PARAMETERS

Panel	a	b	c
$M_g [M_\odot]$	1.8×10^{12}	10^{12}	1.2×10^{12}
r_{hl}	$13.75''$	$13.75''$	$13.75''$
e_g	0	0.2	0.2
β_g	2	2.2	2.2
κ_g	1.3×10^{-2}	3.8×10^{-3}	4.2×10^{-3}
$M_h [M_\odot]$	4.6×10^{15}	1.9×10^{15}	4.9×10^{14}
c_{vir}	9.6	4.7	24
r_h	$127''$	$194''$	$24''$
e_h	0	0.2	0.15
β_h	0.4	1	0
κ_h	0.576	0.166	1.33

Note. — Parameters for the models of Abell 383 shown in Figure 1. We use $z_l = 0.189$, $z_s = 1.0$ in a flat Λ CDM cosmology with $\Omega_M = 0.3$ and $h = 0.7$. Quoted halo masses are virial masses, where the virial overdensity is approximated using the fitting formula of Bryan & Norman (1998). Concentrations are defined by $c_{vir} = r_{vir}/r_h$.

constraints.

After the completion of this paper, we became aware of independent work by Bartelmann & Meneghetti (2003), who reach similar conclusions.

2. ANALYSIS

2.1. Data and models

The observables modeled by S03 are the lensing critical radii (basically the radii of the tangential and radial arcs) and the velocity dispersion profiles of the brightest cluster galaxies; the data are given in their Tables 4–5. For

a given mass model, the critical radii are determined by projecting the density distribution and locating the singular points of the lens mapping (see e.g. Schneider et al. 1992), while the velocity dispersion profile is computed by solving the spherical Jeans equation (see appendix).

We use a generalization of the two-component mass model used by S03. For the stellar component, we use the η model (Tremaine et al. 1994),

$$\rho_{gal} = \frac{(3 - \beta_g)M_g}{4\pi r_g^3} \left[\left(\frac{r}{r_g} \right)^{\beta_g} \left(1 + \frac{r}{r_g} \right)^{4 - \beta_g} \right]^{-1}. \quad (1)$$

S03 mainly used a Jaffe model, which is a particular case of the η model with $\beta_g = 2$. Following S03, we describe the dark matter with a generalized NFW-type profile,

$$\rho_{DM} = \frac{M_h}{4\pi r_h^3 f(c_{vir})} \left[\left(\frac{r}{r_h} \right)^{\beta_h} \left(1 + \frac{r}{r_h} \right)^{3 - \beta_h} \right]^{-1}, \quad (2)$$

where $f(c) = \int_0^c x^{2 - \beta_h} / (1 + x)^{3 - \beta_h} dx$.

2.2. A case study: Abell 383

In the S03 results Abell 383 provided the strongest evidence that the dark matter slope is shallower than r^{-1} , so we use this cluster to study important systematic uncertainties in the analysis. If we center both the stellar and dark matter models on the observed central galaxy position, orient them along the observed galaxy position angle, and fix the stellar model’s half-light radius to the observed galaxy effective radius ($13.75''$), then the remaining model parameters are: the galaxy mass, inner slope, and ellipticity (M_g, β_g, e_g); and the halo mass, scale radius, inner slope, and ellipticity (M_h, r_h, β_h, e_h). S03 used a spherical Jaffe model for the stellar component ($\beta_g = 2$ and $e_g = 0$), and a spherical halo ($e_h = 0$) with scale radius $r_h = 400$ kpc. With the same assumptions, we reproduce their constraints on the dark matter inner slope β_h .

The surface brightness profile of the central galaxy, shown by Smith et al. (2001), is steeper than expected for a Jaffe model and so we adopt $\beta_g \approx 2.2$, however we note that this steep slope has been disputed (R. Ellis 2003, private communication). We find that with this stellar component the models can accommodate a somewhat steeper dark matter profile: with a $\beta_g = 2$ galaxy the best-fit halo has $\beta_h \approx 0.38$, while with $\beta_g = 2.2$ it shifts to $\beta_h \approx 0.45$. The shift of $\Delta\beta_h \lesssim 0.1$ is comparable to various systematic effects considered by S03. The model with a $\beta_g = 2.2$ galaxy fits better than the S03 model (with $\Delta\chi^2 = -1.5$), so henceforth we focus on it.

A larger effect is associated with the dark matter scale radius. The S03 constraints on β_h depend crucially on their assumption of $r_h = 400$ kpc, because there is a degeneracy between r_h and the dark matter slope β_h . For example, assuming $r_h = 200$ kpc would yield $\beta_h \approx 0.18$, while assuming $r_h = 800$ kpc would yield $\beta_h \approx 0.66$ (for spherical models). The latter model fits considerably better than the S03 model ($\Delta\chi^2 = -2.6$), even though S03 claimed that $\beta_h > 0.55$ was excluded at 99% confidence. For spherical models, larger β_h do require large scale radii r_h : for example, the best-fitting model with $\beta_h = 0.8$ has $r_h > 1$ Mpc! Such implausibly large scale radii (or small concentrations) would suggest that steep

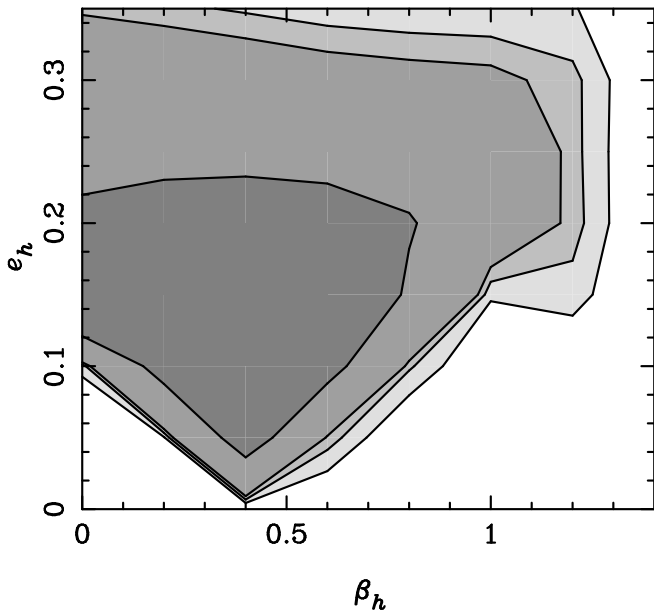


FIG. 2.— Constraints on dark matter inner slope β_h and ellipticity e_h for Abell 383. Contours are drawn at the 68, 90, 95 and 99% confidence levels.

cusps are still disfavored, but that is very different from claiming that steep cusps are inconsistent with the data. The lesson is that r_h must be treated as a free parameter, while keeping in mind that its value should be checked *a posteriori* for plausibility.

The most dramatic effects arise upon dropping the assumption of spherical symmetry. The ellipticity of the galaxy is not exceedingly important; we use the observed value $e_g = 0.2$ and find that it does not significantly change the results. What matters most is the ellipticity of the halo. Figure 2 shows likelihood contours in the plane of e_h and β_h , optimizing over the other parameters (M_g , M_h , and r_h). We find that a broad range of dark matter slopes are consistent with the data. In the limit of spherical symmetry we recover the tight constraints on β_h found by S03, but if we allow even a relatively small ellipticity we find successful models over the range $0 < \beta_h < 1.4$. Thus, the limits found by S03 appear to be an artifact of their prior assumptions for the mass model, notably the assumption of spherical symmetry. Note that the models we find with steeper inner slopes ($\beta \approx 1$) have perfectly sensible parameters from a theoretical standpoint. For example, model b in Table 1, with a $\beta_h = 1$ cusp, has galaxy mass $M_g = 10^{12} M_\odot$, halo mass $M_h = 1.9 \times 10^{15} M_\odot$, and a halo scale radius $r_h = 610$ kpc, corresponding to a concentration of $c_{\text{vir}} = 4.7$. These halo parameters are fully consistent with the virial masses and concentrations expected for hot ($T = 7.1$ keV) X-ray luminous clusters. (Note that with moderate ellipticities it is possible to have $\beta_h = 1$ without an unphysically large scale radius.)

2.3. Additional constraints: MS 2137–23

The case of Abell 383 suggests that simply combining the lensing critical radii with dynamical data cannot strongly constrain the dark matter slope. Fortunately, the use of more detailed lensing data and modeling can

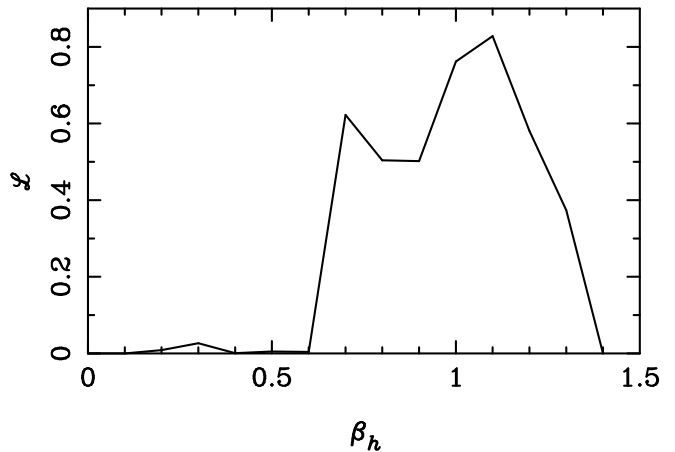


FIG. 3.— Likelihood as a function of the dark matter slope β_h in MS 2137–23, based on lensing, X-ray temperature, and dynamics.

provide constraints on the ellipticity that significantly improve the constraints on the dark matter slope. To illustrate, we consider MS 2137–23. While S03 used only the lensing critical radii, Gavazzi et al. (2003) identified multiple images of 26 distinct sources in the arcs produced by this cluster, enabling much more detailed modeling. Additionally, the X-ray temperature has been measured to be $T = 5.56$ keV (Allen et al. 2001), which can provide constraints on the halo mass via the M – T relation determined by Allen et al. (2001) for relaxed lensing clusters. We combine these data with the velocity dispersions from S03, but we inflate the positional error bars on the multiply imaged knots reported by Gavazzi et al. to $1''$, and inflate the error on the X-ray temperature to 1 keV, in order to maximize the impact of the velocity dispersions on the fit. (We neglect the 5th image claimed by Gavazzi et al., as its detection is tentative.)

We again use two-component mass models, assuming the galaxy and dark matter halo to be concentric. We use the observed values of the galaxy half-light radius ($5.02''$), ellipticity ($e_g = 0.17$), and position angle. If we force the halo to be spherical and to have scale radius $r_h = 400$ kpc we recover the same constraints on β_h as S03. However, if we allow the dark matter halo parameters to vary and optimize over them (and also over the galaxy mass M_g), we find the likelihood as a function of the dark matter slope β_h shown in Figure 3. The dark matter slope is constrained to be $\beta_h = 1 \pm 0.35$ (95% confidence). This is quite consistent with the results found by Gavazzi et al., which perhaps is not too surprising: since we found earlier that the velocity dispersion data are not terribly restrictive, it is reasonable that the joint constraints from dynamics and detailed lens modeling are similar to those obtained from lens modeling alone. Typical halo virial masses and concentrations obtained were roughly $M_h \sim 7 \times 10^{14} M_\odot$ and $c_{\text{vir}} \sim 7$. Incidentally, we find that mild halo ellipticities ($e_h \sim 0.2$) and mild misalignment between halo and galaxy ($\Delta\theta \lesssim 10^\circ$) are favored by the fits.

3. DISCUSSION

We have argued that the stringent constraints claimed by Sand et al. (2003) on the inner slope of the dark mat-

ter profiles in clusters — $\beta_h = 0.38 \pm 0.06$ for Abell 383, $\beta_h = 0.57 \pm 0.11$ for MS 2137–23 — are not supported by their data. We have found successful models with dark matter slopes well outside these bounds. The models with steep slopes ($\beta_h \approx 1$) have sensible parameters: halo virial masses $M_h \sim 10^{15} M_\odot$ and concentrations $c_{\text{vir}} \approx 4$ –5.

It appears that the tight constraints obtained by S03 on the inner dark matter profile are artifacts of several simplifying assumptions in their modeling analysis. We have shown that the assumption of spherical symmetry and of a particular value of the halo scale radius artificially restricts the range of parameters consistent with the data. It may seem surprising that small departures from sphericity (e.g., ellipticities $e \sim 0.1$ –0.2) generate such striking differences in the lensing properties of the clusters. However, as discussed by Dalal et al. (2003) and Bartelmann & Meneghetti (2003), the strong lensing cross section for objects with shallow radial profiles is highly sensitive to small shear perturbations, arising for example from ellipticity. In other words, small changes in ellipticity elicit large changes in the size of the critical curves for lenses with shallow profiles. This extra degree of freedom in the models thwarts any attempts to derive tight constraints on the density profiles from the critical radii alone.

The lack of strong constraints does not mean that lensed arcs are not useful probes of the inner structure of cluster dark matter halos. We have also shown that detailed modeling of lensed features and dynamics does allow interesting constraints to be placed on the inner potential. Decomposing the central mass distribution in MS 2137–23 into stellar and dark matter components, we found constraints on the dark matter inner slope of $\beta = 1 \pm 0.35$ at 95% confidence.

We wouldn't take this measurement too seriously, though. First, we have not fully explored the model parameter space — considering tidal shear from nearby ha-

los or substructures within the cluster, or a radially varying ellipticity, could weaken the bounds on β_h . Second, it can be argued that decomposing the total mass into stellar and dark matter components, which is a standard approach, is not ideal. Because the effects of baryonic mass on the dark matter distribution are poorly understood, the dark matter profile obtained by subtracting the baryonic component from the total mass might be very different from the profile the dark matter would have assumed in the absence of baryonic interference. For example, Loeb & Peebles (2003) have suggested that the decomposition procedure could give the appearance of a cored dark matter distribution, even for proper CDM halos.

Thus, as with galaxy rotation curves, probing the dark matter on scales dominated by baryons is a perilous exercise. A much better test of CDM predictions would be to measure the profile on scales that are DM dominated. Fortunately, giant arcs offer such a probe, since they occur on scales (~ 50 –100 kpc) beyond the influence of central galaxies, yet well inside the $\rho \propto r^{-\beta}$ regime expected in clusters. Simple measurements of lensing critical radii are not enough, however; detailed lens modeling is required. Fortunately, the data to support such modeling are available, and several clusters have already yielded interesting (and in some cases surprising) measurements of their dark matter distributions (e.g., Gavazzi et al. 2003; Kneib et al. 2003).

We thank many colleagues for their encouragement, including Rennan Barkana, Avi Loeb, David Rusin, and Joop Schaye. N. D. and C. R. K. acknowledge the support of NASA through Hubble Fellowship grants HST-HF-01148.01-A and HST-HF-01141.01-A awarded by the Space Telescope Science Institute, which is operated by the Association of Universities for Research in Astronomy, Inc., for NASA, under contract NAS 5-26555.

APPENDIX

Here we discuss the calculation of the velocity dispersion and lensing properties of the mass models defined in §2.1. For spherically symmetric distributions with isotropic velocity dispersion tensors, the spherical Jeans equations are solved by (Binney & Tremaine 1987)

$$\sigma^2(r) = \frac{1}{\rho(r)} \int_r^\infty \rho(r') \frac{GM(r')}{r'^2} dr', \quad (1)$$

where $\rho(r)$ is the stellar density, G is Newton's constant and $M(r)$ is the total (stellar+DM) mass interior to radius r . This velocity dispersion is not directly observed; instead the projected, luminosity-weighted dispersion is measured. Assuming a constant mass-to-light ratio, this becomes

$$\sigma_p^2(R) = \frac{\int_R^\infty \rho(r) \sigma^2(r) \frac{r}{\sqrt{r^2 - R^2}} dr}{\int_R^\infty \rho(r) \frac{r}{\sqrt{r^2 - R^2}} dr} = \frac{2}{\Sigma(R)} \int_R^\infty \rho(r) \frac{GM(r)}{r^2} \sqrt{r^2 - R^2} dr, \quad (2)$$

where $\Sigma(r)$ is the projected surface density. Averaging over a finite radial bin from R_1 to R_2 gives

$$\sigma_{\text{bin}}^2(R_1, R_2) = \frac{\int_{R_1}^{R_2} \sigma_p^2(R) \Sigma(R) dR}{\int_{R_1}^{R_2} \Sigma(R) dR} = \frac{\frac{1}{2} \int_{R_1}^{R_2} \rho(r) GM(r) \left[F\left(\frac{R_2}{r}\right) - F\left(\frac{R_1}{r}\right) \right] dr}{\int_{R_1}^{R_2} r \rho(r) \left[A\left(\frac{R_2}{r}\right) - A\left(\frac{R_1}{r}\right) \right] dr}, \quad (3)$$

where

$$A(x) = \begin{cases} \sin^{-1}(x) & x < 1 \\ \frac{\pi}{2} & x > 1 \end{cases} \quad \text{and} \quad F(x) = \begin{cases} x\sqrt{1-x^2} + \sin^{-1}(x) - \frac{\pi}{2} & x < 1 \\ 0 & x > 1 \end{cases}$$

For the density profiles we have employed, of the form

$$\rho(x = r/r_s) = \frac{\rho_s}{x^\beta (1+x)^{n-\beta}}, \quad (4)$$

there are no closed-form expressions for the projected surface density in terms of elementary functions. The convergence $\kappa = \Sigma/\Sigma_{\text{crit}}$ takes the form (e.g., Wyithe et al. 2001)

$$\kappa(u = R/r_s) = 2\kappa_s u^{1-\beta} \int_0^{\pi/2} \frac{(\sin \theta)^{n-2}}{(u + \sin \theta)^{n-\beta}} d\theta, \quad (5)$$

where $\kappa_s = \rho_s r_s / \Sigma_{\text{crit}}$ and as usual Σ_{crit} is the lensing critical surface density. For elliptical surface density profiles with axis ratio $q = 1 - e$, we use $\kappa(\sqrt{x^2 + y^2/q^2})$ with $\kappa_s = \rho_s r_s / (q \Sigma_{\text{crit}})$. Keeton (2001) discusses how the deflection angle and distortion tensor may be expressed as one-dimensional integrals over κ and its derivatives. The ellipticities of interest to us are small enough ($e \sim 0.1$ – 0.2 in the density, even smaller in the potential) that we assume it is a reasonable approximation to use the spherical Jeans equations to compute the line-of-sight velocity dispersion (Kochanek 1994).

REFERENCES

- Allen, S. W., Schmidt, R. W., & Fabian, A. C. 2001, *MNRAS*, 328, L37
- Athreya, R. M., Mellier, Y., van Waerbeke, L., Pelló, R., Fort, B., & Dantel-Fort, M. 2002, *A&A*, 384, 743
- Bartelmann, M. & Meneghetti, M. 2003, submitted to *A&A*, astro-ph/0312011
- Binney, J. & Tremaine, S. 1987, *Galactic dynamics* (Princeton, NJ, Princeton University Press, 1987, 747 p.)
- Blumenthal, G. R., Faber, S. M., Flores, R., & Primack, J. R. 1986, *ApJ*, 301, 27
- Bryan, G. L. & Norman, M. L. 1998, *ApJ*, 495, 80
- Clowe, D. & Schneider, P. 2002, *A&A*, 395, 385
- Dahle, H. 2003, *ArXiv Astrophysics e-prints*, astro-ph/0310549
- Dalal, N., Holder, G., & Hennawi, J. 2003, *ArXiv Astrophysics e-prints*, astro-ph/0310306
- Dutton, A. A., Courteau, S., Carignan, C., & de Jong, R. 2003, *ArXiv Astrophysics e-prints*, astro-ph/0310001
- El-Zant, A., Hoffman, Y., Primack, J., Combes, F., & Shlosman, I. 2003, *ArXiv Astrophysics e-prints*, astro-ph/0309412
- Gavazzi, R., Fort, B., Mellier, Y., Pelló, R., & Dantel-Fort, M. 2003, *A&A*, 403, 11
- Keeton, C. R. 2001, *ArXiv Astrophysics e-prints*, astro-ph/0102340
- Kelson, D. D., Zabludoff, A. I., Williams, K. A., Trager, S. C., Mulchaey, J. S., & Bolte, M. 2002, *ApJ*, 576, 720
- Kneib, J., Hudelot, P., Ellis, R. S., Treu, T., Smith, G. P., Marshall, P., Czoske, O., Smail, I., & Natarajan, P. 2003, *ApJ*, in press, astro-ph/0307299
- Kochanek, C. S. 1994, *ApJ*, 436, 56
- Loeb, A. & Peebles, P. J. E. 2003, *ApJ*, 589, 29
- Moore, B., Governato, F., Quinn, T., Stadel, J., & Lake, G. 1998, *ApJ*, 499, L5+
- Navarro, J. F., Frenk, C. S., & White, S. D. M. 1997, *ApJ*, 490, 493
- Navarro, J. F., Hayashi, E., Power, C., Jenkins, A., Frenk, C. S., White, S. D. M., Springel, V., Stadel, J., & Quinn, T. R. 2003, *ArXiv Astrophysics e-prints*, astro-ph/0311231
- Sand, D. J., Treu, T., & Ellis, R. S. 2002, *ApJ*, 574, L129
- Sand, D. J., Treu, T., Smith, G. P., & Ellis, R. S. 2003, *ArXiv Astrophysics e-prints*, astro-ph/0300703 (S03)
- Schneider, P., Ehlers, J., & Falco, E. E. 1992, *Gravitational Lenses* (Gravitational Lenses, XIV, 560 pp. 112 figs.. Springer-Verlag Berlin Heidelberg New York. Also *Astronomy and Astrophysics Library*)
- Simon, J. D., Bolatto, A. D., Leroy, A., & Blitz, L. 2003, *ApJ*, 596, 957
- Smith, G. P., Kneib, J., Ebeling, H., Czoske, O., & Smail, I. 2001, *ApJ*, 552, 493
- Tremaine, S., Richstone, D. O., Byun, Y., Dressler, A., Faber, S. M., Grillmair, C., Kormendy, J., & Lauer, T. R. 1994, *AJ*, 107, 634
- Wyithe, J. S. B., Turner, E. L., & Spergel, D. N. 2001, *ApJ*, 555, 504